Check for updates

Experimental validation of eosin-mediated photo-redox polymerization mechanism and implications for signal amplification applications†

Emma H. Yee,[a] Seunghyeon Kim [ID] [a] and Hadley D. Sikes [ID] *[a,b,c]

Oxygen-tolerant radical polymerization has demonstrated applications in biosensors as a signal amplification method for molecular recognition events. In particular, eosin-mediated photo-redox polymerization, a visible light-initiated radical copolymerization method using *N*-vinyl pyrrolidone and PEDGA monomers, can be performed in aqueous microliter-scale droplets under atmospheric conditions, and has been used for rapid (≤90 s) signal amplification in several diagnostic assays. In recent years, significant progress has been made in understanding the reaction mechanism, and here we assess the accuracy of the proposed mechanism *via* experimental validation in an assay format. A 2D reaction–diffusion model was developed and compared to experimental behavior of eosin photopolymerization for paper-based signal amplification. For 3 and 4 mm test zones, the model predicted, within an order of magnitude, experimentally observed effects of oxygen exposure and eosin photoinitiator concentration on polymer formation in a droplet. Both model and experimental results demonstrated that high oxygen exposure and low eosin concentration restrict polymer formation to the center of circular wells. Decreasing the surface-area-to-volume ratio of the reaction droplet and increasing eosin concentration allow polymerization throughout the zone, initially forming in radially intermediate zones due to oxygen's role not just as a reaction inhibitor but also a promoter *via* photoinitiator regeneration. Reaction volumes as low as 20 μL on 3, 4, and 5 mm diameter reaction zones enabled sensitive signal amplification, although higher oxygen exposure (3–10 μL droplets) showed greatly reduced sensitivity. Observing oxygen tolerance limits and experimentally validating the reaction mechanism can help better understand the eosin photopolymerization system and its applications in diagnostic assay signal amplification.

[a]*Department of Chemical Engineering, Massachusetts Institute of Technology, Cambridge, MA 02139, USA*
[b]*Program in Polymers and Soft Matter, Massachusetts Institute of Technology, Cambridge, MA 02139, USA*
[c]*Antimicrobial Resistance Interdisciplinary Research Group, Singapore-MIT Alliance for Research and Technology, 1 CREATE Way, Singapore 138602.*
E-mail: sikes@mit.edu
†Electronic supplementary information (ESI) available: Includes model equations, variables, and initial conditions, materials, eosin conjugation and imaging methods, and supplementary model *vs.* experimental results. See DOI: 10.1039/d1py00413a

Introduction

Radical polymerization, where radical species react with hundreds to millions of monomers to generate a polymer, has demonstrated potential in recent years as a method for signal amplification in biosensors.[1–11] Biosensors detect the presence of target biomolecules by capturing them with nucleic acids or proteins and converting that specific biodetection event into a measureable signal. This signal generation is often achieved by coupling a label to another nucleic acid or protein that recognizes the captured molecules. In methods such as atom-transfer radical polymerization (ATRP),[2] reversible addition–fragmentation chain transfer (RAFT),[4] redox-initiated free radical polymerization,[5,6] and photoinitiated free radical polymerization,[7,12–14] that label is an initiator, chain transfer agent, or catalyst involved in either initiation or propagation so that polymerization will occur only if sufficient quantities of these labels are present due to specific target molecule capture events. The variety of initiation reactions and monomer choices give this amplification method versatility and flexibility as a signal amplification method in sensing and detection applications.

Many oxygen tolerant methods of performing ATRP,[8] RAFT,[9–11] redox-mediated polymerization,[3] and photoinitiated polymerization[15–19] have been demonstrated, enhancing their ability for use in many laboratory-based and point-of-care assays. In particular, visible light-initiated free radical polymerization with eosin Y (eosin dianion) and a tertiary

amine has been used as a rapid, low-cost signal amplification method to detect biomarkers of several infectious diseases.[16,20–23] In eosin photopolymerization, the absorption of a photon of wavelength in the vicinity of 517 nm excites eosin into a triplet intermediate state where it can undergo electron transfer with a triethanolamine (TEOA) coinitiator.[24,25] The electron donation to eosin's triplet excited state *via* a loosely bound charge-transfer complex yields an eosin radical trianion and a TEOA radical cation[26] (Fig. 1A). TEOA radical cations either decay to TEOA radicals, which propagate the radical polymerization of monomers, or react with oxygen to form stable iminium cations and superoxide.[27] Eosin radical trianions can also react with oxygen to regenerate eosin dianion (Fig. 1A). Like most radical polymerization reactions, eosin photopolymerization is inhibited by oxygen, which hinders propagation by forming peroxy radicals which are less reactive than carbon-centered free radicals. For polymerization to occur at ambient conditions, a small amount of free eosin Y is added to the monomer solution[15] such that oxygen is sufficiently scavenged by eosin radical trianion and TEOA radical cation species in solution.[27,28] However, oxygen also plays a uniquely promotional role by regenerating eosin *via* oxidation of eosin radical trianions, allowing the photoinitiation process to continue even with low concentrations of eosin photoinitiator.

TEOA radicals catalyze the copolymerization of polyethylene glycol diacrylate (PEGDA) and N-vinylpyrrolidone (VP). VP is commonly employed in acrylate photopolymerization reactions to reduce oxygen inhibition and enhance the rate of radical polymerization and final conversion.[25,27,29,30]

When used for signal amplification, eosin photoinitiators are coupled to nucleic acids[16,22] or proteins[16,20,21,23] that specifically recognize captured biomarkers. Local photoinitiator concentration will increase when biodetection events occur, and polymer forms when the local concentration exceeds the minimum initiator threshold where propagation reactions become competitive with inhibition reactions. Polymer formation can enable a colorimetric readout through the use of the pH indicating dye, phenolphthalein, in the monomer solution. Eosin photopolymerization has been previously used as an amplification method for colorimetric detection in diagnostic tests for tuberculosis,[20,22] malaria,[21] and periodontal disease.[23]

A thorough understanding of the reaction kinetics and reaction mechanism of eosin photopolymerization promotes its effective use for signal amplification. An ability to predict how polymerization is affected by changes in geometry or changes in key species like inhibitory oxygen and eosin photoinitiator is crucial in understanding how the signal amplification method can best be applied.

Models have previously been developed to study eosin-mediated photopolymerization at ambient conditions,[25,31,32] and some even hypothesized a regeneration mechanism for eosin.[31–33] Many insights into the eosin regeneration mechanism have since been made,[26,28,34] but have yet to be combined into a kinetic model and validated with experimental results in actual diagnostic test conditions.

Here, we developed a 2D axisymmetric reaction–diffusion model to simulate diagnostic test conditions where a droplet of monomer solution is applied to a paper biodetection zone and irradiated with green light for photoinitiated signal amplification. The reaction–diffusion system models polymerization throughout the droplet, initiated by the free eosin Y in the monomer solution rather than by bound initiators at the
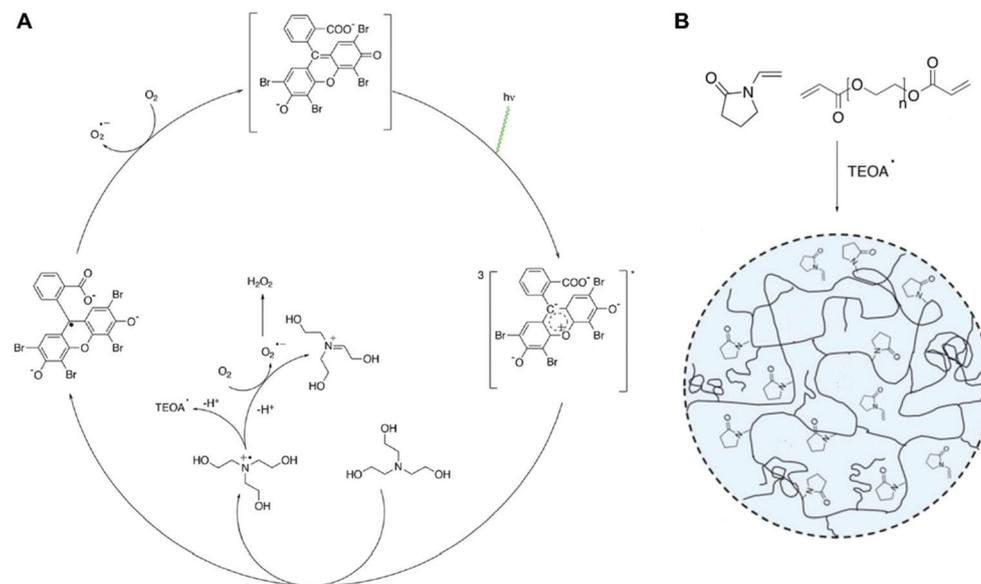

Fig. 1 (A) Role of oxygen in eosin and triethanolamine co-initiator radical formation, termination, and regeneration. Adapted from Aguirre-Soto *et al.*, *Polym. Chem.*, 2019, **10**(8), 926. (B) Copolymerization of PEGDA and VP by triethanolamine radicals produced in (A).

sensing interface. It did not incorporate surface-immobilized eosin that occurs in molecular recognition events. The model incorporated key reactions in the proposed mechanism and solved for species concentration throughout the system over time. The model's predictions of when and where in the test zone polymer forms were compared with experimental results. The effects on polymer formation of changing eosin Y photo-initiator concentration and oxygen exposure in the monomer solution were investigated. We then investigated if the model's predicted trends for solution-phase polymerization behavior could also be used to predict and understand polymer formation in biodetection assays where eosin-conjugated streptavidin was captured on paper-based tests by an engineered binding protein.

Experimental

Eosin photopolymerization experimental setup

A Xerox ColorQube solid ink printer was used to pattern Whatman No. 1 chromatography paper, which was then exposed to 150 °C for 1 minute to melt the ink through the paper to define hydrophilic, circular wells (3, 4, and 5 mm diameter) as test zones. A monomer solution was prepared, composed of 200 mM polyethylene glycol diacrylate (PEGDA), 100 mM *N*-vinyl pyrrolidinone (VP), 150 mM triethanolamine (TEOA), 1.6 mM phenolphthalein, 0.02 *N* hydrochloric acid, and varying amounts of eosin Y (0.3–0.5 μM). As described previously,[23] eosin photopolymerization was performed by applying a 20 μL droplet of monomer solution to the test zone and irradiating with 25 mW cm^{-2}, 522 nm light supplied by an ampliPHOX reader. The zone was then washed with DI water and a 2 μL droplet of 0.5 M sodium hydroxide was added to visualize any phenolphthalein-containing polymer that formed.

Test zones were imaged with an iPhone 7 camera. Because ambient lighting and operator positioning affect image color,[35] those variables were controlled in the setup. The smartphone was clamped a set distance directly above the test well to be imaged. Lighting conditions were controlled by imaging in a windowless room with constant overhead lighting in a ceiling-less box of white paper to minimize glare.

Reaction–diffusion model

A system of reaction diffusion equations and boundary conditions were modeled using COMSOL Multiphysics software, numerically solved using backward differentiation formula (BDF) and parallel direct solver (PARDISO) with a maximum time step of 0.1 s and total reaction time of 200 s. The droplet was approximated as a cylinder, which was solved as a 2D axisymmetric geometry. The cylinder volume was always identical to the experimental droplet volume it was meant to simulate (20 μL or 3 μL/10 μL for shallow droplets). The geometry was discretized into a mesh with 0.1 mm maximum mesh spacing.

The following conservation equation was numerically solved at each mesh point.

$$\frac{\partial c_i}{\partial t} + \nabla J_i = R_i$$

$$J_i = -D_i \nabla c_i.$$

Species balances were solved for each chemical species using reaction terms from the rate equations in the kinetic reaction mechanism. All reactions included in the model, kinetic rate constants, diffusion coefficients, and other parameters were listed in ESI.† To simulate oxygen exposure to droplets at ambient conditions, a flux boundary condition was applied at all outer surfaces of the model using an approximation of Fick's Law at each surface point in the mesh. Here, $c_{O_2,0}$ is the initial dissolved oxygen concentration in the monomer solution.[34] The approximate oxygen boundary layer size, δ, was set to 0.1 mm.[36]

$$J_{O_2} = -D_{O_2} \frac{c_{O_2,0} - c_{O_2}(t)}{\delta}.$$

Initial concentration of eosin and all other monomer components in the model was set identical to experimental conditions with which it was compared (see ESI†).

Gelation time ($t_{0.2}$)

Double bond conversion, or the amount of monomer double bonds reacted scaled to its initial amount, is one property that denotes the extent of polymerization. In this system initiated by eosin and a tertiary amine, 20% conversion is approximately when gelation occurs and the solution begins to solidify.[28,37] Experimentally, $t_{0.2}$ was defined as the irradiation time necessary for pink polymer to form on the test zone. In the model, $t_{0.2}$ was defined as the time when double bond conversion reached 20% anywhere in the model. Measuring $t_{0.2}$ was one way polymerization response to changes in initiator concentration and oxygen exposure was assessed.

Creating biodetection assays

The reaction–diffusion model created here simulates solution-phase polymerization throughout the droplet, and therefore initial experimental validation of the model was performed by looking at polymer response due to eosin initiators present in low concentrations in the monomer solution. However, in practice, when eosin photopolymerization is used for signal amplification, the test zone will contain eosin bound to the surface if the target molecule has been captured. After initial validation of the model, we performed eosin photopolymerization with actual assays that captured eosin-conjugated streptavidin to determine if the trends observed in our model would apply to biodetection applications.

The biodetection assay was created by first immobilizing cellulose binding domain (CBD)-rcSso7d streptavidin binder constructs.[38] We previously engineered a charge-neutralized variant of the *Sulfolobus solfataricus* DNA binding protein, rcSso7d, to specifically bind streptavidin. Fusing it to CBD

enables rapid, high efficiency immobilization of the binder on cellulose paper.[38,39] Eosin-5-isothiocyanate was conjugated to streptavidin (ESI†) and applied to the assay for specific molecular capture that could be detected *via* eosin photopolymerization.

Results and discussion

Predicting spatial polymer formation with the reaction–diffusion model

The reaction–diffusion model was first developed as a 3 mm diameter cylinder with 20 µL volume to mimic experimental conditions of polymerization in 20 µL droplets on 3 mm diameter paper test zones (Fig. 2A). As a cylinder with uniform boundary conditions is axisymmetric, the model was solved as a rectangular 2D slice that captured species concentration and values over time throughout the 3D cylinder (Fig. 2B). These model "slices" are used in the figures of this paper to more easily visualize model outputs at various time points. In all these "slices" the left boundary is the center of the cylinder "droplet" and the three other boundaries are directly exposed to the air.

In examining the model, we looked not only at concentration of monomer solution species and double bond conversion over time, but also at the Damköhler number (Da_{O_2}), a ratio of oxygen reaction rate to diffusion rate throughout the droplet. This helps understand what is happening to oxygen throughout the droplet over time.

$$Da_{O_2} = \frac{\text{rate of O}_2 \text{ reaction}}{\text{rate of O}_2 \text{ diffusion}}.$$

Like experimental results (Fig. 2C), the model predicts that under the set conditions, the highest rates of double bond formation and initial polymer formation occur in intermediate areas not at the droplet center but also not at the edge (Fig. 2D). Why conversion is highest in the area can be explained by the roles of oxygen in the system. While oxygen plays a major inhibitory role in the eosin photopolymerization reaction, it also reacts with eosin radicals to regenerate eosin. Polymerization can only occur when oxygen concentration is essentially zero, but that polymerization also relies on the eosin regenerated by oxygen to form initiating TEOA radicals. For this reason we see that the area when oxygen first drops to zero (Fig. 2E) is also the area where oxygen is reacting the fastest (high Da_{O_2}) (Fig. 2F), regenerating eosin that then
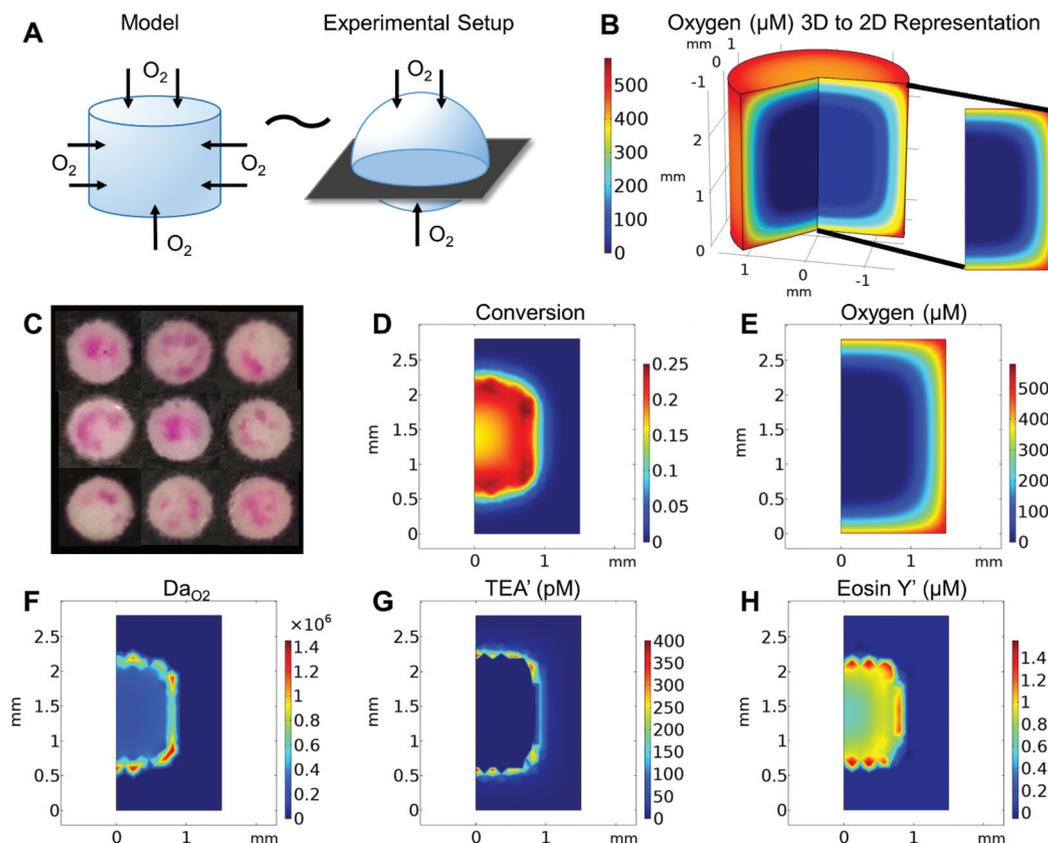

Fig. 2 (A) A cylindrical model geometry was used to mimic the droplet used in paper-based assays. (B) Due to its axisymmetric nature, the 3D model space could be described by 2D slices showing spatial concentrations and ratios over time. (C) Experimental and (D) model results show that initial polymerization occurs in intermediate zones close to the (E) oxygen diffusion front. The (F) oxygen Damköhler number, and concentration of (G) tertiary amine radicals and (H) eosin radicals can help understand this phenomenon.

reacts with TEOA to form high concentrations of TEOA and eosin Y radicals (Fig. 2G and H).

Effects of eosin concentration on polymerization

We then examined the effects of varying eosin photoinitiator concentration on polymer formation. In both the model and experiments, the eosin concentration was varied from 0.3 to 0.5 μM and its effects on time to gelation ($t_{0.2}$) and spatial polymer formation were observed. This range of eosin concentration was chosen because it has been previously observed that the polymerization reaction is highly sensitive to small changes in eosin, and has a dynamic range around 0.3–0.7 μM.[15] This is largely due to the high photocatalytic efficiency of eosin Y in the presence of oxygen and use of high intensity of light (25 mW cm^{-2}) in this system.

Both the model and experiments found that increasing eosin concentration decreases $t_{0.2}$ and allows polymer to form further from center (Fig. 3). In further validation of our proposed reaction mechanism, the model predicted $t_{0.2}$ quite accurately, and captured its nonlinear dependence on eosin concentration.

Eosin and the TEOA radicals generated by photoinitiation both react with oxygen to deplete it and allow polymerization to occur. Therefore, higher eosin concentrations increase the rate of oxygen depletion, which reduces $t_{0.2}$ and allow oxygen-depleting reactions to occur closer to the oxygen-exposed edge of the droplet. However, the area of highest polymerization rate also moves closer to the droplet edge, following the oxygen diffusion front, as it depends on oxygen to regenerate eosin initiators.

It is important to note that most of the calculated $t_{0.2}$ or "gelation time" is taken up by oxygen inhibition, when radical polymerization cannot occur due to the presence of oxygen in the reaction droplet.[18,27] For example, in modeling the case of 0.4 μM eosin Y (Fig. 3), it took 90 seconds for eosin radical trianion and TEOA radical cation reactions to deplete oxygen completely in at least one point of the volume, but it is 115 seconds before double bond conversion reaches 0.2. Because $t_{0.2}$ is so heavily dependent on oxygen inhibition, the scaling of $t_{0.2}$ with catalyst (eosin) loading is very high and does not appear to follow the usual propagation–initiation rate scaling of free radical polymerization reactions.[40]

Effects of oxygen exposure on polymerization

Understanding how eosin photopolymerization responds to changing assay conditions is helpful in applying it for signal amplification in biodetection methods. We examined how polymer formation was affected when the test zone size was increased from 3 mm to 4 and 5 mm, while keeping the reaction volume the same (20 μL). Larger wells therefore had thinner droplets with higher surface-area-to-volume ratios. Eosin concentration was kept constant at 0.4 μM.

As expected, due to oxygen inhibition, larger test zones with thinner droplets took longer to polymerize and polymerized in an area closer to the well center, as the region where oxygen could be sufficiently depleted by initiators decreased. This was observed both experimentally and from the model (Fig. 4 and Table 1). It was observed experimentally that significantly less polymer formed in 5 mm-diameter wells (Fig. 4B).

While the model did predict no polymerization (even after 300 s irradiation) for 5 mm-diameter wells, it is likely that radical formation is barely outcompeting oxygen inhibition in the high oxygen exposure conditions of the 5 mm-diameter wells, and the model margin of error prevented accurate pre-
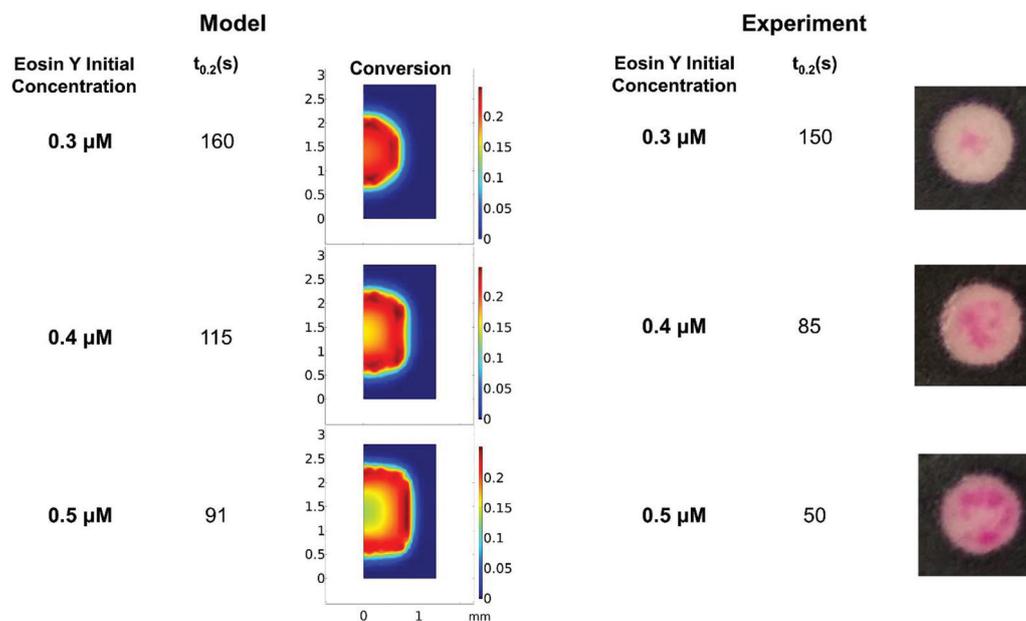

Fig. 3 In both model and experimental results, increasing eosin Y concentration increased the area in which polymer will form and reduced the irradiation time necessary to form polymer.
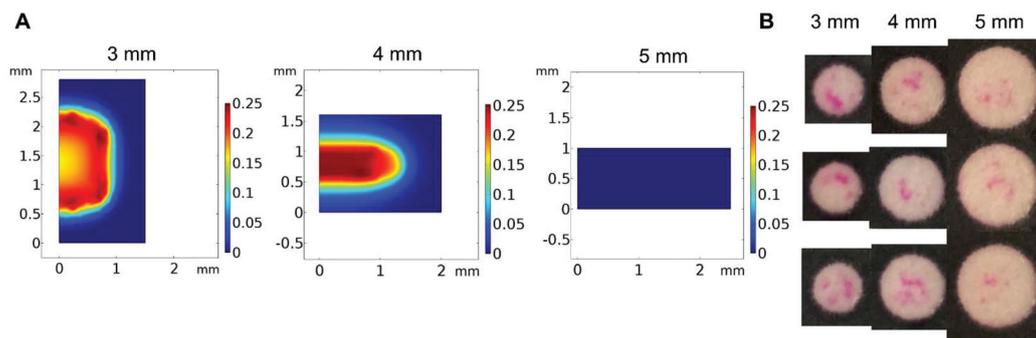
Fig. 4 Model predictions and experimental effects of increasing test zone diameter and droplet surface-area-to-volume ratio.

Table 1 Experimental vs. model predicted gelation time

Well diameter (mm)	3	4	5
Experimental $t_{0.2}$ (s)	85	95	105
Model predicted $t_{0.2}$ (s)	115	157	Never

diction in an environment so close to total inhibition. The model could be made more accurate by approximating the droplet as an ellipsoid and measuring more kinetic parameters for the system rather than using approximations from literature. We used sensitivity analysis to quantify the impact of possible inaccuracies in several rate constants and the oxygen boundary layer (Fig. S1†). For example, we calculated that $t_{0.2}$ would decrease by 5% if k_{isc} in our system is 10% larger than the literature value. However, in spite of these approximations, the model accurately predicted trends in polymer spatial and temporal formation with well diameter and oxygen exposure of reaction droplets.

Effects of oxygen exposure on polymerization amplification in biodetection assays

We first investigated experimental and model results focused on polymerization in settings where eosin is not immobilized on the test zone surface. However, when eosin photopolymerization is used in practice for signal amplification, the zone is irradiated for a time just below $t_{0.2}$, such that when no biodetection events take place, visible polymerization will not occur. Only when eosin is bound to the zone surface due to biodetection events does the eosin concentration increase such that polymerization will occur within a time frame less than $t_{0.2}$.

To simulate actual biodetection applications of eosin photopolymerization and determine if the trends observed in our model would apply to this scenario, biodetection assays were created by immobilizing streptavidin-binding proteins on 3, 4, and 5 mm test zones and capturing eosin-conjugated streptavidin. Volumes of capture binder and streptavidin eosin were adjusted depending on the test zone size such that all test sizes and all replicates had approximately the same surface concentration of eosin (Fig. S2†). Eosin photopolymerization was then used for signal amplification on test

zones of various sizes, all with 20 μL monomer solution droplets. Zones were irradiated for a time 5 seconds below $t_{0.2}$ such that negative samples (no immobilized streptavidin binder) returned no polymer.

In this biodetection format, the same trends previously predicted by the model and observed experimentally were also seen. As the test zone diameter increases, and the droplet volume becomes more exposed to oxygen, polymer formation becomes restricted to areas closer to the droplet center (Fig. 5).

Polymerization in very thin droplets

To probe the extent of oxygen tolerance in eosin photopolymerization, we next examined polymerization in very thin droplets: 3 μL for 3 mm zones and 10 μL for 5 mm zones. The model predicted that even after 200 s of irradiation, polymerization will not occur under experimental conditions. Experimental results also demonstrated this behavior, with no polymer forming even after 200 s of irradiation (Fig. S3†). This demonstrates that polymerization throughout the droplet, initiated by the free eosin Y in the monomer solution rather than by bound initiators at the sensing interface, can be completely inhibited when droplets reach a certain thinness and solution-phase eosin concentration is insufficient to consume oxygen before it diffuses throughout the droplet.

In some cases, it could be advantageous to use shallow droplets that are not sensitive to photoactivation (irradiation) time, and can be irradiated for long periods of time without risk of false positives, or formation of colored polymer due to the free eosin Y in the monomer solution, not due to biorecognition events. However, shallow droplets would be useful only for assays where high sensitivity is not required. Here, it was observed that high oxygen exposure in very shallow droplets greatly reduced sensitivity to molecular recognition events (Fig. 6). Eosin photopolymerization was again performed on biodetection assay test zones where eosin-streptavidin had been specifically captured at a uniform surface concentration for both 3 mm and 5 mm diameter zones. However, this time, 3 μL and 10 μL monomer solution was applied to the zones, respectively. Both 3 mm and 5 mm-diameter zones demonstrated greatly reduced polymer response when a smaller droplet of monomer solution was applied.
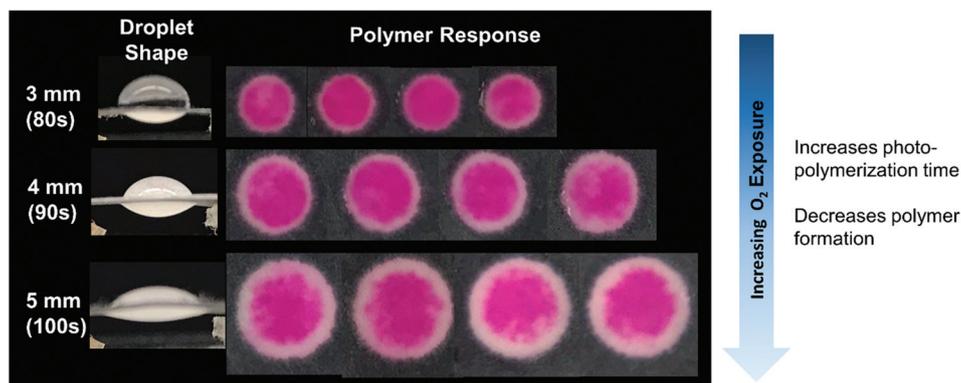
Fig. 5 Eosin photopolymerization for signal amplification in biodetection assays of varied reaction zone diameter and droplet shape (all droplets were 20 µL in volume). Increasing droplet oxygen exposure led to increased time needed for polymerization and decreased polymer formation.
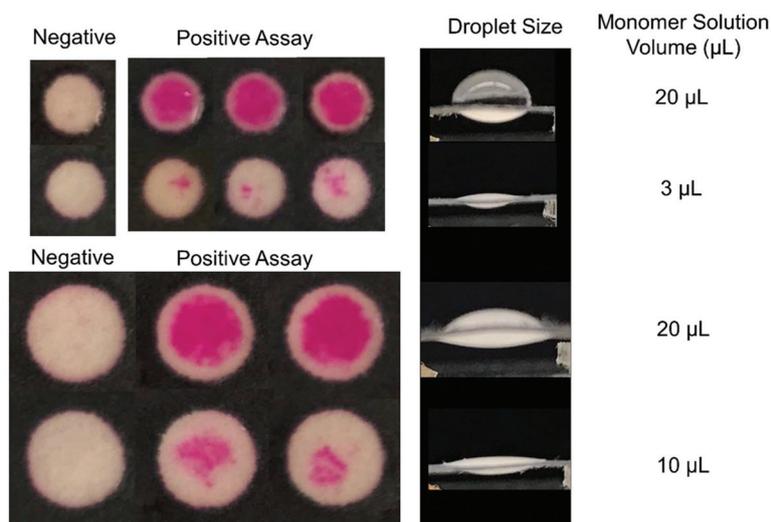

Fig. 6 Signal amplification sensitivity of eosin photopolymerization in 3 and 5 mm biodetection assays was greatly decreased when very shallow reaction droplets were used.

When eosin photopolymerization is used to amplify signal from eosin-coupled biodetection events, it is a threshold process: polymer forms when local concentration of eosin photoinitiator exceeds the minimum initiator threshold (due to macrophotoinitiator-linked molecular recognition events) where propagation reactions become competitive with inhibition reactions. For maximum sensitivity, the reaction with added solution-based initiator and no surface-bound eosin should be very close to that threshold, such that even a small number of surface molecular recognition events that bind eosin to the zone surface will bump the initiator concentration over the threshold. It is evident that under conditions of high oxygen exposure, the system is not at all close to that threshold, and lots of initiator must first be immobilized before polymerization can occur—greatly reducing sensitivity.

These results can guide application of eosin photopolymerization, and other radical polymerization reactions, in paper-based diagnostic assays. A variety of platforms exist, such as lateral and vertical flow assays, where solutions flow via capillary action through paper channels where reactions occur. Sliding chip assays, where paper reaction zones are manually slid in and out of fluidic paths to enable incubation with reagent droplets, have also been proposed. Another format that allows for reactions to occur in droplets is 96-well printed sheets,[41] similar to traditional 96-well plates commonly used for ELISA and other high-throughput screening assays.

The results presented in this paper indicate that eosin photopolymerization sensitivity is promoted in monomer droplets with lower surface-area-to-volume ratios, which minimize oxygen exposure. This indicates that eosin photopolymerization signal amplification is most applicable in assay platforms where droplets of at least 10 s of µL are feasible, such as high throughput screening assays in 96-well printed

formats. For more portable, point-of-care applications, devices like sliding chip assays,[42] where solutions can be localized in small areas, could be compatible with this amplification method. This is likely also true for other oxygen-inhibited radical polymerization reactions that can be performed at ambient conditions, such as enzyme- and redox pair-mediated free radical polymerization,[1,3] and some modified forms of ATRP[8] and RAFT.[9–11]

Eosin photopolymerization and other radical polymerization methods would likely be incompatible with flow-through formats (lateral and vertical flow assays) where monomer solutions would be highly exposed to oxygen.[43] It is possible that radical polymerization could work in flow-through formats for assays targeting molecules in such high abundance that low sensitivity is acceptable. Additionally, in some cases, greatly increasing initiator concentration or light intensity could overcome inhibitory reactions.

Conclusions

A reaction–diffusion model was developed for eosin-mediated photo-redox polymerization that accurately predicts experimentally observed polymer gelation times and polymer response within an order of magnitude. This level of accuracy enables tuning of the reaction and droplet geometry to meet time and sensitivity needs. Given that the model only used main reactions in the mechanism, and relied on approximations of some kinetic rate constants, model accuracy could be even further improved by adding more reactions and/or measuring more kinetic rate constants.

Trends observed in model and experimental results demonstrate that careful consideration of assay platform compatibility with radical polymerization reactions—even relatively oxygen-tolerant ones—is necessary when determining if or how radical polymerization can be applied for signal amplification. While this paper specifically investigated eosin-mediated photo-redox polymerization reactions, its conclusions regarding the effects of oxygen exposure and initiator concentration on spatial polymer formation and sensitivity could be generalized to many other oxygen-inhibited free radical polymerization reactions, such at various ATRP, RAFT, and redox-initiated radical polymerization methods, which are only oxygen tolerant to a certain point. While concentration of initiator or other methods of suppressing oxygen inhibition can be varied for specific reaction conditions, in some applications radical polymerization may not allow achievement of desired sensitivity and/or reaction speed. This work illustrates the value of appropriately matching signal amplification chemistry to the desired assay format and performance needs.

Author contributions

The paper was written through contributions of all authors.

Conflicts of interest

The authors declare no Conflict of interest.

Acknowledgements

References

1 S. Kim and H. D. Sikes, Radical Polymerization Reactions for Amplified Biodetection Signals, *Polym. Chem.*, 2020, **11**(8), 1424–1444, DOI: 10.1039/c9py01801h.

2 K. Matyjaszewski and J. Xia, Atom Transfer Radical Polymerization, *Chem. Rev.*, 2001, **101**(9), 2921–2990, DOI: 10.1021/cr940534g.

3 A. J. Gormley, R. Chapman and M. M. Stevens, Polymerization Amplified Detection for Nanoparticle-Based Biosensing, *Nano Lett.*, 2014, **14**(11), 6368–6373, DOI: 10.1021/nl502840h.

4 C. L. McCormick and A. B. Lowe, Aqueous RAFT Polymerization: Recent Developments in Synthesis of Functional Water-Soluble (Co)Polymers with Controlled Structures, *Acc. Chem. Res.*, 2004, **37**(5), 312–325, DOI: 10.1021/ar0302484.

5 A. S. Sarac, Redox Polymerization, *Prog. Polym. Sci.*, 1999, **24**(8), 1149–1204, DOI: 10.1016/S0079-6700(99)00026-X.

6 S. R. Zavada, T. Battsengel and T. F. Scott, Radical-Mediated Enzymatic Polymerizations, *Int. J. Mol. Sci.*, 2016, **17**(2), 195, DOI: 10.3390/ijms17020195.

7 Y. Yagci, S. Jockusch and N. J. Turro, Photoinitiated Polymerization: Advances, Challenges, and Opportunities, *Macromolecules*, 2010, **43**(15), 6245–6260, DOI: 10.1021/ma1007545.

8 K. Min, W. Jakubowski and K. Matyjaszewski, AGET ATRP in the Presence of Air in Miniemulsion and in Bulk, *Macromol. Rapid Commun.*, 2006, **27**(8), 594–598, DOI: 10.1002/marc.200600060.

9 D. Liu, W. Cai, L. Zhang, C. Boyer and J. Tan, Efficient Photoinitiated Polymerization-Induced Self-Assembly with Oxygen Tolerance through Dual-Wavelength Type i Photoinitiation and Photoinduced Deoxygenation, *Macromolecules*, 2020, **53**(4), 1212–1223, DOI: 10.1021/acs.macromol.9b02710.

10 J. Peng, Q. Xu, Y. Ni, L. Zhang, Z. Cheng and X. Zhu, Visible Light Controlled Aqueous RAFT Continuous Flow Polymerization with Oxygen Tolerance, *Polym. Chem.*, 2019, **10**(16), 2064–2072, DOI: 10.1039/c9py00069k.

11 T. Zhang, J. Yeow and C. Boyer, A Cocktail of Vitamins for Aqueous RAFT Polymerization in an Open-to-Air Microtiter

Plate, *Polym. Chem.*, 2019, **10**(34), 4643–4654, DOI: 10.1039/c9py00898e.

12 C. A. Figg, J. D. Hickman, G. M. Scheutz, S. Shanmugam, R. N. Carmean, B. S. Tucker, C. Boyer and B. S. Sumerlin, Color-Coding Visible Light Polymerizations to Elucidate the Activation of Trithiocarbonates Using Eosin Y, *Macromolecules*, 2018, **51**(4), 1370–1376, DOI: 10.1021/acs.macromol.7b02533.

13 M. D. Thum, S. Wolf and D. E. Falvey, State-Dependent Photochemical and Photophysical Behavior of Dithiolate Ester and Trithiocarbonate Reversible Addition-Fragmentation Chain Transfer Polymerization Agents, *J. Phys. Chem. A*, 2020, **124**(21), 4211–4222, DOI: 10.1021/acs.jpca.0c02678.

14 Y. Zhao, M. Ma, X. Lin and M. Chen, Photoorganocatalyzed Divergent Reversible-Deactivation Radical Polymerization towards Linear and Branched Fluoropolymers, *Angew. Chem., Int. Ed.*, 2020, **59**(48), 21470–21474, DOI: 10.1002/anie.202009475.

15 K. Kaastrup and H. D. Sikes, Polymerization-Based Signal Amplification under Ambient Conditions with Thirty-Five Second Reaction Times, *Lab Chip*, 2012, **12**(20), 4055, DOI: 10.1039/c2lc40584a.

16 L. R. Kuck and A. W. Taylor, Photopolymerization as an Innovative Detection Technique for Low-Density Microarrays, *BioTechniques*, 2008, **45**(2), 179–186, DOI: 10.2144/000112889.

17 M. L. Allegrezza and D. Konkolewicz, PET-RAFT Polymerization: Mechanistic Perspectives for Future Materials, *ACS Macro Lett.*, 2021, **10**, 433–446, DOI: 10.1021/acsmacrolett.1c00046.

18 C. Wu, H. Chen, N. Corrigan, K. Jung, X. Kan, Z. Li, W. Liu, J. Xu and C. Boyer, Computer-Guided Discovery of a PH-Responsive Organic Photocatalyst and Application for PH and Light Dual-Gated Polymerization, *J. Am. Chem. Soc.*, 2020, **141**(20), 8207–8220, DOI: 10.1021/jacs.9b01096.

19 B. Nomeir, O. Fabre and K. Ferji, Effect of Tertiary Amines on the Photoinduced Electron Transfer-Reversible Addition-Fragmentation Chain Transfer (PET-RAFT) Polymerization, *Macromolecules*, 2019, **52**(18), 6898–6903, DOI: 10.1021/acs.macromol.9b01493.

20 K.-J. Sung, H. D. Sikes, Y. Jabbour, A. Maalouf, Q. R. Johns and E. A. Miller, Functional Comparison of Paper-Based Immunoassays Based on Antibodies and Engineered Binding Proteins, *Analyst*, 2020, **145**, 2515–2519, DOI: 10.1039/d0an00299b.

21 A. K. Badu-Tawiah, S. Lathwal, K. Kaastrup, M. Al-Sayah, D. C. Christodouleas, B. S. Smith, G. M. Whitesides and H. D. Sikes, Polymerization-Based Signal Amplification for Paper-Based Immunoassays, *Lab Chip*, 2015, **15**(617), 655–659, DOI: 10.1039/C4LC01239A.

22 E. H. Yee and H. D. Sikes, Polymerization-Based Amplification for Target-Specific Colorimetric Detection of Amplified Mycobacterium Tuberculosis DNA on Cellulose, *ACS Sens.*, 2020, **5**(2), 308–312, DOI: 10.1021/acssensors.9b02424.

23 E. H. Yee, S. Lathwal, P. P. Shah and H. D. Sikes, Detection of Biomarkers of Periodontal Disease in Human Saliva Using Stabilized, Vertical Flow Immunoassays, *ACS Sens.*, 2017, **2**, 1589–1593, DOI: 10.1021/acssensors.7b00745.

24 M. V. Encinas, A. M. Rufs, S. G. Bertolotti and C. M. Previtali, Xanthene Dyes/Amine as Photoinitiators of Radical Polymerization: A Comparative and Photochemical Study in Aqueous Medium, *Polymer*, 2009, **50**(13), 2762–2767, DOI: 10.1016/j.polymer.2009.04.024.

25 S. Kizilel, V. H. Pérez-Luna and F. Teymour, Mathematical Model for Surface-Initiated Photopolymerization of Poly (Ethylene Glycol) Diacrylate, *Macromol. Theory Simul.*, 2006, **15**(9), 686–700, DOI: 10.1002/mats.200600030.

26 A. Aguirre-Soto, K. Kaastrup, S. Kim, K. Ugo-Beke and H. D. Sikes, Excitation of Metastable Intermediates in Organic Photoredox Catalysis: Z-Scheme Approach Decreases Catalyst Inactivation, *ACS Catal.*, 2018, **8**(7), 6394–6400, DOI: 10.1021/acscatal.8b00857.

27 A. Aguirre-Soto, S. Kim, K. Kaastrup and H. D. Sikes, On the Role of: N-Vinylpyrrolidone in the Aqueous Radical-Initiated Copolymerization with PEGDA Mediated by Eosin y in the Presence of O 2, *Polym. Chem.*, 2019, **10**(8), 926–937, DOI: 10.1039/c8py01459k.

28 K. Kaastrup, A. Aguirre-Soto, C. Wang, C. N. Bowman, J. W. Stansbury and H. D. Sikes, UV-Vis,/FT-NIR in Situ Monitoring of Visible-Light Induced Polymerization of PEGDA Hydrogels Initiated by Eosin/Triethanolamine/O2, *Polym. Chem.*, 2016, **7**(3), 592–602, DOI: 10.1039/c5py01528f.

29 T. J. White, W. B. Liechty and C. A. Guymon, The Influence of N-Vinyl Pyrrolidone on Polymerization Kinetics and Thermo-Mechanical Properties of Crosslinked Acrylate Polymers, *J. Polym. Sci., Part A: Polym. Chem.*, 2007, **45**, 4062–4073, DOI: 10.1002/pola.

30 Y. Hao, H. Shih, Z. Munoz, A. Kemp and C.-C. Lin, Visible Light Cured Thiol-Vinyl Hydrogels with Tunable Degradation for 3D Cell Culture, *Acta Biomater.*, 2014, **10**(1), 104–114, DOI: 10.1016/j.actbio.2013.08.044.Visible.

31 C. Deeb, C. Ecoffet, R. Bachelot, J. Plain, A. Bouhelier and O. Soppera, Plasmon-Based Free-Radical Photopolymerization: Effect of Diffusion on Nanolithography Processes, *J. Am. Chem. Soc.*, 2011, **133**, 10535–10542, DOI: 10.1021/ja201636y.

32 J. Wong and H. D. Sikes, The Impact of Continuous Oxygen Flux in a Thin Film Photopolymerization Reaction with Peroxy-Mediated Regeneration of Initiator, *Macromol. Theory Simul.*, 2016, **25**(3), 229–237, DOI: 10.1002/mats.201500098.

33 H. J. Avens and C. N. Bowman, Mechanism of Cyclic Dye Regeneration during Eosin-Sensitized Photoinitiation in the Presence of Polymerization Inhibitors, *J. Polym. Sci., Part A: Polym. Chem.*, 2009, **47**(22), 6083–6094, DOI: 10.1002/pola.23649.

34 J. Wong, K. Kaastrup, A. Aguirre-Soto and H. D. Sikes, A Quantitative Analysis of Peroxy-Mediated Cyclic Regeneration of Eosin under Oxygen-Rich Photopolymerization Conditions, *Polymer*, 2015, **69**, 169–177, DOI: 10.1016/j.polymer.2015.05.043.

35 J. Schwiegerling, *Field Guide to Visual and Ophthalmic Optics*, SPIE Press, Bellingham, WA, 2004.

36 G. N. Nishihara and J. D. Ackerman, On the Determination of Mass Transfer in a Concentration Boundary Layer, *Limnol. Oceanogr.: Methods*, 2007, **5**(2), 88–96, DOI: 10.4319/lom.2007.5.88.

37 G. V. Korolev and M. M. Mogilevich, *Three-Dimensional Free-Radical Polymerization*, Springer Berlin Heidelberg, Berlin, 2009.

38 E. A. Miller, S. Baniya, D. Osorio, Y. Jabbour, A. Maalouf and H. D. Sikes, Paper-Based Diagnostics in the Antigen-Depletion Regime : High-Density Immobilization of RcSso7d-Cellulose-Binding Domain Fusion Proteins for e Ffi Cient Target Capture, *Biosens. Bioelectron.*, 2018, **102**(August 2017), 456–463.

39 E. A. Miller, M. W. Traxlmayr, J. Shen and H. D. Sikes, Activity-Based Assessment of an Engineered Hyperthermophilic Protein as a Capture Agent in Paper-Based Diagnostic Tests, *Mol. Syst. Des. Eng.*, 2016, **1**(4), 377–381, DOI: 10.1039/c6me00032k.

40 G. Moad, *Radical Polymerization, Reference Module in Materials Science and Materials Engineering*, Elsevier, 2016.

41 R. C. Murdock, L. Shen, D. K. Gri, N. Kelley-loughnane, I. Papautsky and J. A. Hagen, Optimization of a Paper-Based ELISA for a Human Performance Biomarker, *Anal. Chem.*, 2013, **85**, 11634–11642.

42 J. T. Connelly, J. P. Rolland and G. M. Whitesides, "Paper Machine" for Molecular Diagnostics, *Anal. Chem.*, 2015, **87**(15), 7595–7601, DOI: 10.1021/acs.analchem.5b00411.

43 J. E. Schonhorn, S. C. Fernandes, A. Rajaratnam, R. N. Deraney, J. P. Rollanda and C. R. Mace, A Device Architecture for Three-Dimensional, Patterned Paper Immunoassays, *Lab Chip*, 2014, **14**(24), 4653–4658, DOI: 10.1039/c4lc00876f.